1 ## *De novo* synthesis of phosphatidylcholine is essential for the promastigote but
2 ## not amastigote stage in *Leishmania major*

3

4 Samrat Moitra[a], Somrita Basu[a], Mattie Pawlowic[a*], Fong-fu Hsu[b] and Kai Zhang[a#]

5

6 [a]Department of Biological Sciences, Texas Tech University, Lubbock, TX 79409, USA.

7

8 [b]Mass Spectrometry Resource, Division of Endocrinology, Diabetes, Metabolism, and Lipid
9 research, Department of Internal Medicine, Washington University School of Medicine, St.
10 Louis, MO 63110, USA.

11

12 *Current address: Biological Chemistry and Drug Discovery, Wellcome Centre for Anti-
13 Infectives Research (WCAIR), University of Dundee, Dundee, UK.

14

15 #Corresponding author: Kai Zhang, Department of Biological Sciences, Texas Tech University,
16 Lubbock, TX 79409, USA. Tel: 1-806-834-0550. E-mail: kai.zhang@ttu.edu.

17

18 Short title: How do *Leishmania* make PC?

ABSTRACT

Phosphatidylcholine (PC) is the most abundant type of phospholipids in eukaryotes constituting ~30% of total lipids in *Leishmania*. PC synthesis mainly occurs via the choline branch of the Kennedy pathway (choline $\Rightarrow$ choline-phosphate $\Rightarrow$ CDP-choline $\Rightarrow$ PC) and the N-methylation of phosphatidylethanolamine (PE). In addition, *Leishmania* parasites can acquire PC and other lipids from the host or culture medium. In this study, we assessed the function and essentiality of choline ethanolamine phosphotransferase (CEPT) in *Leishmania major* which is responsible for the final step of the *de novo* synthesis of PC and PE. Our data indicate that CEPT is localized in the endoplasmic reticulum and possesses the activity to generate PC from CDP-choline and diacylglycerol. Targeted deletion of *CEPT* is only possible in the presence of an episomal *CEPT* gene in the promastigote stage of *L. major*. These chromosomal null parasites require the episomal expression of *CEPT* to survive in culture, confirming its essentiality during the promastigote stage. In contrast, during *in vivo* infection of BALB/c mice, these chromosomal null parasites appeared to lose the episomal copy of *CEPT* while maintaining normal levels of virulence, replication and cellular PC. Therefore, while the *de novo* synthesis of PC/PE is indispensable for the proliferation of promastigotes, intracellular amastigotes appear to acquire most of their lipids through salvage and remodeling.

INTRODUCTION

Leishmaniasis is caused by protozoan parasites of the genus *Leishmania* which alternate between extracellular promastigotes colonizing the midgut of sandflies and intracellular amastigotes residing in the macrophage of mammals (Alvar et al., 2012). Without a safe vaccine, the mitigation of leishmaniasis mainly depends on vector control and drugs (Croft and Olliaro, 2011). Current therapeutics are limited and plagued with high toxicity (Croft and Olliaro, 2011). A better understanding of how *Leishmania* parasites acquire essential cellular components may lead to new drug targets and improved treatments.

Glycerophospholipids such as phosphatidylcholine (PC) and phosphatidylethanolamine (PE) are among the most abundant types of lipids accounting for approximately 30% and 10% of total lipids in *Leishmania*, respectively (Zhang and Beverley, 2010; Zheng et al., 2010). While PC in promastigotes primarily consists of 1,2-diacyl-PC, the majority of leishmanial PE belongs to 1-O-alk-1′-enyl-2-acyl-*sn*-glycero-3-phosphoethanolamine or plasmenylethanolamine (PME) (Beach et al., 1979; Zufferey et al., 2003; Pawlowic et al., 2016; Moitra et al., 2019). Due to its positively charged head group, PC is a membrane-forming phospholipid that is more abundant on the outer leaflet of the plasma membrane (van Meer et al., 2008; Nickels et al., 2015). Meanwhile, PE is known for its ability to promote membrane fusion and mainly resides in the inner leaflet (Verkleij et al., 1984; Ellens et al., 1989; Zachowski, 1993). Besides being principal membrane components, PC and PE possess other important functions. For example, PC can serve as the precursor for a number of important signaling molecules and metabolic intermediates including lyso-PC, phosphatidic acid, diacylglycerol (DAG) and free fatty acids (FA) (Exton, 1994; Furse and de Kroon, 2015). In addition, PE is required for the synthesis of GPI-anchored proteins in trypanosomatids by providing the ethanolamine (EtN) phosphate bridge that links proteins to glycan anchors (Menon et al., 1993). PE also contributes to the formation of autophagosome during differentiation and starvation (Ichimura et al., 2000; Besteiro et al., 2006; Williams et al., 2012) and the posttranslational modification of eukaryotic elongation factor 1A in trypanosomatids (Signorell et al., 2008a). Thus, understanding the mechanism by which *Leishmania* acquire their PC and PE may reveal new ways to block their growth.

In many eukaryotic cells, the majority of PE and PC are synthesized *de novo* via the Kennedy pathway (Kennedy, 1956; Cui and Vance, 1996; Gibellini and Smith, 2010). As indicated in Fig. 1, the *de novo* synthesis of PE, i.e. the EtN branch of the Kennedy pathway, starts with the phosphorylation of EtN into EtN-phosphate, which is also generated from the metabolism of sphingoid bases (Zhang et al., 2007); EtN-phosphate is then conjugated to CTP by ethanolaminephosphate cytidylyltransferase (EPCT) to produce CDP-EtN and pyrophosphate; and two enzymes catalyze the final steps: an ethanolamine phosphotransferase (EPT) which combines CDP-EtN with 1-alkyl-2-acyl-glycerol to form the precursor of PME (Pawlowic et al., 2016) (Fig. 1), and a choline ethanolamine phosphotransferase (CEPT) which condenses CDP-EtN and DAG into diacyl-PE (Fig. 1). A parallel route, aka the choline branch of the Kennedy pathway, is responsible for the *de novo* synthesis of PC (choline → choline-phosphate → CDP-choline → PC, Fig. 1), and CEPT catalyzes the last step of combining CDP-choline and DAG into PC as a dual activity enzyme (Henneberry and McMaster, 1999; Signorell et al., 2008b; Vance, 2008).

3

83

84   In addition to *de novo* synthesis, PE and PC are also generated from the conversion of

85 phosphatidylserine (PS) and the N-methylation of PE, respectively (Fig. 1). Furthermore,

86 *Leishmania* can scavenge glycerophospholipids and degrade them via the activity of

87 phospholipase A2 (PLA2), suggesting that these parasites can remodel exogenous lipids into

88 their own via the Lands cycle (Das et al., 2001; Henriques et al., 2003; Parodi-Talice et al., 2003;

89 Castanys-Munoz et al., 2007; Pawlowic and Zhang, 2012) (Fig. 1). Because the Kennedy

90 pathway is the dominant route for PE/PC synthesis in most eukaryotes including *Trypanosoma*

91 *brucei* (a trypanosomatid parasite related to *Leishmania*) (Signorell et al., 2008b; Gibellini and

92 Smith, 2010), we have examined the roles of several genes involved in this pathway in

93 *Leishmania major*. First, to explore the significance of PME production, we generated the *EPT*-

94 null mutants (*ept*⁻) which were largely devoid of PME but contained WT-levels of diacyl-PE

95 (Pawlowic et al., 2016). *Ept*⁻ promastigotes were fully viable and replicative in culture but

96 showed significantly attenuated virulence in mice (Pawlowic et al., 2016). Meanwhile, *ept*⁻

97 amastigotes were fully virulent, indicating that PME synthesis alone was not required during the

98 mammalian stage for *L. major* (Pawlowic et al., 2016). Second, to determine the role of *de*

99 *novo* PC synthesis in *L. major*, we focused on the cholinephosphate cytidylyltransferase (CPCT)

100 which catalyzes the choline-phosphate to CDP-choline conversion in the choline branch of the

101 Kennedy pathway (Fig. 1). Without CPCT, *L. major* parasites could not incorporate choline into

102 PC, yet the *CPCT*-null promastigotes (*cpct*⁻) contained similar levels of PC and PE as WT

103 parasites in culture (Moitra et al., 2019). Loss of *CPCT* did not affect promastigote replication in

104 complete media but caused reduced growth rates under EtN-limiting conditions (Moitra et al.,

105 2019). Both *cpct*⁻ promastigotes and amastigotes were fully virulent in mice (Moitra et al.,

106 2019). Collectively, these observations suggest that other routes of PC synthesis (e.g., PE N-

107 methylation and lipid salvage) can compensate the loss of CPCT (Fig. 1).

108

109   In this study, we investigated the function of CEPT in *L. major* which is expected to

110 directly catalyze the formation of diacyl-PC and diacyl-PE via the Kennedy pathway (Fig. 1). In

111 *T. brucei*, RNAi knockdown of CEPT significantly reduced the biosynthesis of PE and PC and

112 caused a cytokinesis defect resulting in the accumulation of zoids (Signorell et al., 2008b;

113 Signorell et al., 2009). These findings are in agreement with the dual substrate activity exhibited

114 by *T. brucei* CEPT (Farine et al., 2015). Given the fact that CPCT is not essential for *L. major*, it

115 is important to probe whether the *de novo* PC synthesis is required for *Leishmania* promastigotes

116 and amastigotes. Unlike *T. brucei* which has separate Kennedy pathway branches for PE and PC

117 synthesis (Gibellini and Smith, 2010; Smith and Butikofer, 2010), *Leishmania* parasites can

118 incorporate EtN into both PE and PC (Pawlowic et al., 2016; Moitra et al., 2019), presumably

119 through the activity of PE-N-methyltransferases (Bibis et al., 2014). Thus, CEPT is likely

120 required for the synthesis of PC through both the Kennedy pathway and the methylation of PE in

121 *Leishmania* (Fig. 1). Our results demonstrate that CEPT is indispensable for *L. major*

122 promastigotes but not amastigotes, suggesting that intracellular parasites can fulfill their need for

123 PC through lipid salvage/remodeling.

4

MATERIALS AND METHODS

Materials

For the CEPT activity assay, [methyl-^{14}C] CDP-choline (50–60 mCi/mmol) and [diarachidonyl-1-^{14}C] PC (50–60 mCi/mmol) were purchased from Perkin Elmer, Inc (Waltham, MA) and American Radiolabeled Chemicals (St. Louis, MO), respectively. 1,2-Dioctanoyl-sn-glycerol (DAG) was purchased from EMD Millipore (Burlington, MA). Lipid standards for mass spectrometry including 1,2-dimyristoyl-*sn*-glycero-3-phosphoethanolamine (14:0/14:0-PE) and 1,2-dimyristoyl-*sn*-glycerol-3-phosphocholine (14:0/14:0-PC) were purchased from Avanti Polar Lipids (Alabaster, AL). All other reagents were purchased from Thermo Fisher Scientific (Hampton, NH) unless specified otherwise.

Molecular constructs

The open reading frame (ORF) of *CEPT* (LmjF36.5900) was amplified by PCR from *L. major* genomic DNA and cloned into the pXG vector (Ha et al., 1996) to generate pXG-*CEPT*. The *CEPT* ORF was then subcloned into the pXG-GFP' (Ha et al., 1996) and pXNG4 vectors (Murta et al., 2009) to generate pXG-*GFP-CEPT* and pXNG4-*CEPT*, respectively. The upstream and downstream flanking sequences (~1 Kb each) of *CEPT* were PCR amplified and cloned in tandem into the pUC18 vector. Genes conferring resistance to puromycin (*PAC*) and blasticidin (*BSD*) were inserted between the upstream and downstream flanking sequences to generate pUC18-KO-*CEPT:PAC* and pUC18-KO-*CEPT:BSD*, respectively. All the molecular constructs were confirmed by restriction enzyme digestion and sequencing. Oligo nucleotides used in this study are summarized in Table S2.

Leishmania culture and genetic manipulation

L. major LV39 clone 5 (Rho/Su/59/P) promastigotes were cultivated at 27 ºC in M199 media with 10% heat-inactivated fetal bovine serum and other supplements as previously described (Kapler et al., 1990). To monitor cell growth, promastigotes were inoculated at 1.0-2.0 × 10^5 cells/ml and culture densities were determined over time using a hemocytometer. In general, log phase promastigotes refer to replicative parasites at densities lower than 1.0 × 10^7 cells/ml and stationary phase promastigotes refer to mainly non-replicative parasites at 2.0-3.0 × 10^7 cells/ml. The proliferation of promastigotes from 1.0-2.0 × 10^5 cells/ml to 2.0-3.0 × 10^7 cells/ml (usually in 2-3 days) is referred to as one passage.

To delete *CEPT*, antibiotic resistance cassettes acquired from pUC18-KO-*CEPT:PAC* and pUC18-KO-*CEPT:BSD* were sequentially introduced into LV39 wild type (WT) parasites and drug selections were performed as previously described (Kapler et al., 1990). With this approach, we were able to generate the heterozygous *CEPT+/-* mutants *(ΔCEPT::PAC/CEPT)* but not the homozygous *cept⁻* mutants *(ΔCEPT::PAC/ΔCEPT::BSD)*. To delete the second chromosomal allele of *CEPT*, the pXNG4-*CEPT* plasmid containing *GFP*, *TK*, *SAT* (nourseothricin resistance) and *CEPT* genes was introduced into *CEPT+/-* parasites. The resulting *CEPT+/- +*pXNG4-*CEPT* cells were transfected with the blasticidin resistance cassette from pUC18-*CEPT-KO:BSD*. Parasite showing resistance to puromycin, blasticidin, and nourseothricin were serially diluted into 96-well plates. The resulting clones were amplified and processed for Southern blot analysis to verify the loss of chromosomal *CEPT* and referred to as *cept⁻+*pXNG4-*CEPT*.

170

Fluorescence microscopy and validation of GFP-*CEPT*

172   Promastigotes expressing GFP-*CEPT* were attached to poly-L-lysine coated coverslips,
173 fixed with 3.7% formaldehyde, and then permeabilized on ice with ethanol. Incubation with
174 rabbit anti-*T. brucei* BiP antiserum (1:1000) was performed at room temperature for 40 min.
175 After washing three times with phosphate-buffered saline (PBS), coverslips were incubated with
176 a goat anti-rabbit-IgG Texas Red (1:2000) antiserum for 40 min. After washing three times with
177 PBS, DNA was stained with 2.5 µg/ml of Hoechst 33342, followed by final three washes with
178 PBS. Coverslips containing cells were mounted on glass slides with Fluormount-G mounting
179 medium and an Olympus BX51 Upright Fluorescence Microscope was used to visualize the
180 expression and localization of GFP-*CEPT*. To quantify the overlap between GFP-*CEPT* and anti-
181 BiP staining, 136 randomly selected cells were analyzed using the Image J JACoP (Just Another
182 Colocalization Plugin) (Table S1) (Bolte and Cordelieres, 2006).

183

184   To detect GFP-*CEPT* by Western blot, *Leishmania* promastigotes were boiled in SDS
185 sample buffer, resolved by SDS-PAGE and probed with a rabbit anti-GFP polyclonal antibody
186 (Life Technologies) followed by a goat anti-rabbit IgG-HRP antibody. To ensure equal loading,
187 blots were probes with an anti-α-tubulin monoclonal antibody followed by a goat anti-mouse
188 IgG-HRP antibody. Signals from Western blot were detected using a FluorChem E system
189 (Protein Simple).

190

CEPT assay and thin layer chromatography (TLC)

192   To examine the CEPT activity in *Leishmania*, log phase promastigotes of WT, *CEPT+/-*
193 *+pXG-CEPT* and WT *+pXG-GFP-CEPT* were harvested by centrifugation, washed twice with
194 PBS, and resuspended in a hypotonic lysis buffer (1 mM of Tris-HCl, 0.1 mM of EDTA, 1 x
195 protease inhibitor cocktail, pH 8) at 5×10^8 cells/ml. Cells were lysed by sonication (Ultrasonic
196 homogenizer Sonic Ruptor 250, medium speed, 30 s x 3 times on ice) and protein concentration
197 in lysate was determined by the BCA assay. Procedure for the CEPT activity assay was adapted
198 from a previously reported method with *Trypanosoma brucei* cells (Farine et al., 2015). Briefly,
199 each 100-µl reaction contained 900 µg of leishmanial protein (from promastigote lysate), 50 µM
200 of [^{14}C] CDP-choline, 50 µM of DAG, 50 mM of Tris pH 8.0, 10 mM of MgCl$_2$, and 0.005% of
201 Tween 20 (w/v). After 1-hour incubation at room temperature, the reaction mix was extracted
202 twice with of 250 µl of 1-butanol. The combined organic fractions were dried under a nitrogen
203 stream and reconstituted in 20 µl of 1-butanol. The aqueous fraction was also saved. Materials
204 from the organic and aqueous fractions were analyzed by one-dimensional TLC on a silica gel 60
205 plate (Merck) using a solvent system composed of chloroform:methanol:acetate:water (25:15:4:2
206 by volumes). [^{14}C] CDP-choline, [^{14}C] 1,2-diarachidonyl PC, and [^{14}C] choline chloride were
207 used in the TLC as markers. Mouse liver homogenate was used as a positive control and boiled
208 *Leishmania* lysates were used as negative controls. After TLC, radioactive signals on the silica
209 gel 60 plate were detected using a Personal Molecular Imager (Bio-Rad).

210

GCV treatment of promastigotes in culture

212   Promastigotes of WT, *CEPT+/- +pXNG4-CEPT* and *cept ⁻+pXNG4-CEPT* were
213 cultivated in complete M199 media in the absence or presence of 50 µg/ml of GCV or 200 µg/ml
214 of nourseothricin (for *CEPT+/- +pXNG4-CEPT* and *cept ⁻+pXNG4-CEPT* only). Every three
215 days, parasites were re-inoculated at 1.0×10^5 cells/ml in fresh media containing the same

216 concentration of GCV or nourseothricin to start a new passage. For every passage, the GFP
217 expression level was determined by flow cytometry at mid-log phase ($3-7 \times 10^6$ cells/ml) using
218 an Attune NxT Acoustic Flow Cytometer. After 16 passages in the presence of 50 μg/ml of
219 GCV, *cept⁻*+pXNG4-*CEPT* parasites were sorted based on their GFP expression levels using a
220 BD Biosciences FACS Aria III Plus Cell Sorter. GFP-high and GFP-low parasites (~50,000
221 each) were sorted directly into complete M199. Parasites showing low GFP expression were
222 serially diluted into 96-well plates. Multiple clones were then selected and their GFP expression
223 levels were determined by flow cytometry (examples are shown in Fig. 5E-G).
224
225 **Quantitative PCR (qPCR) analyses to determine *CEPT* transcript level, parasite loads and**
226 **plasmid copy numbers**
227   To determine the *CEPT* transcript level in WT parasites, total RNA was extracted from
228 log phase promastigotes or lesion-derived amastigotes. 1 μg of RNA was converted into
229 complementary DNA using a high-capacity cDNA conversion kit, followed by qPCR using
230 primers designed for the ORF of *CEPT* or the 28S rRNA gene. The expression level of *CEPT*
231 was normalized to that of 28S rRNA using the comparative Ct approach, also known as the $2^{-\Delta\Delta}$
232 $^{(Ct)}$ method (Livak and Schmittgen, 2001).
233
234   To determine parasite numbers, a standard curve was prepared from the serially diluted
235 genomic DNA samples extracted from WT promastigotes (from 2×10^6 cells to 0.2 cells per
236 reaction). Dilutions were carried out in the presence of salmon sperm DNA as a carrier. QPCR
237 was performed on DNA extracted from promastigotes and amastigotes with primers for the 28S
238 rRNA gene. Parasite numbers were determined using the standard curve.
239
240   To determine pXNG4-*CEPT* copy numbers, a calibration curve was generated by serially
241 diluting pXNG4-*CEPT* plasmid DNA from 2×10^6 molecules to 0.2 molecules per reaction in
242 the presence of salmon sperm DNA. QPCR was performed on DNA extracted from
243 promastigotes and amastigotes using primers for the pXNG4 plasmid. Plasmid copy number per
244 cell was calculated by dividing the total plasmid copy number by the total parasite number. All
245 qPCR reactions were performed in triplicates using the SSO Advanced Universal SYBR Green
246 Supermix (Bio-Rad) in an Applied Biosystems 7300 RT-PCR thermo-cycler.
247
248 **Mouse footpad infection and in vivo GCV treatment**
249   Use of mice in this study was approved by the Animal Care and Use Committee at Texas
250 Tech University. BALB/c mice (female, 8 weeks old) were purchased from Charles River
251 Laboratories International. To assess parasite virulence, stationary phase promastigotes were
252 resuspended in serum free M199 medium and injected into the left hind footpad of BALB/c mice
253 (1.0×10^6 cells/mouse, 10 mice per group). For each group, one half of the mice received GCV
254 treatment at 7.5 mg/kg/day (GCV was prepared in sterile PBS, 0.5 ml per day) through
255 intraperitoneal injection, while the other half received sterile PBS (0.5 ml per day). GCV and
256 PBS treatments started one day post infection and continued for 14 days. Mouse body weights
257 were monitored once a week for three weeks post injection. Footpad lesions were measured
258 weekly using a Vernier caliper. Parasite loads in infected footpads were determined at the
259 indicated times by limiting dilution assay as described previously (Titus et al., 1985) and qPCR
260 as described above. Mice were euthanized via CO_2 asphyxiation when their footpad lesions
261 exceeded 2.5 mm or when secondary infections were detected.

7

Recovery and analyses of promastigotes from infected mice

Amastigotes were isolated from 8-10 weeks infected mice and allowed to convert into promastigotes in complete M199 media in the presence or absence of 200 μg/ml of nourseothricin or 50 μg/ml of GCV. Parasites were then continuously cultivated in media containing the same concentration of nourseothricin or GCV. During each passage, the growth rate and GFP expression were determined by cell counting and flow cytometry as described above.

Lipid analysis by electrospray ionization mass spectrometry (ESI-MS)

Total lipids from log phase promastigotes, lesion-derived amastigotes, or uninfected mouse tissue were extracted using the Bligh-Dyer method (Bligh and Dyer, 1959; Zhang, 2012). Purification of lesion amastigotes was performed as previously described (Glaser et al., 1990; Zhang, 2012). Identification of PC, PE and TAG structures using low-energy collision induced dissociation LIT MS^n with high-resolution Fourier transform mass spectrometry was conducted on a Thermo Scientific LTQ Orbitrap Velos mass spectrometer (R=100,000 at m/z 400) with Xcalibur operating system as previously described (Hsu et al., 2014). Fatty acyl constituents and numbers of double bonds in PC, PE and TAG were given when possible. For example, a16:0/16:0 PC represents 1-O-hexadecyl-2-palmitoyl-sn-glycero-3- phosphocholine, e18:0/18:2-PE represents 1-O-octadec-1′-enyl-2-octadecadienoyl-sn-glycero-3-phosphoethanolamine, 36:4 PC represents a 1,2-diacyl-sn-glycero-3-phosphocholine in which the total number of carbon from sn-1 and sn-2 is 36 and the total number of C=C double bonds from sn-1 and sn-2 is 4, and 52:3 TAG represents a TAG in which the total number of carbon from sn-1 to sn-3 is 52 and the total number of C=C double bonds is 3.

Statistical analysis

Unless otherwise specified, all experiments were repeated three times and each biological repeat contained 2–3 technical repeats. Differences among experimental groups were determined by the unpaired Student's t test (for two groups) or one-way ANOVA (for three to four groups) using Sigmaplot 13.0 (Systat Software Inc, San Jose, CA). P values indicating statistical significance were grouped into values of <0.05 (*), <0.01 (**) and <0.001 (***).

RESULTS

Targeted deletion of the endogenous *CEPT* alleles in *L. major*

L. major CEPT is encoded by a single copy gene on chromosome 36 (TritrypDB ID: LmjF36.5900) with well conserved, syntenic orthologs among other trypanosomatids. The predicted protein contains 417 amino acids with 6 transmembrane helices showing 30-33% identity to the CEPTs from organisms outside of kinetoplastids. To investigate the function of this enzyme in *L. major*, we first tried to generate the *CEPT*-null mutants using a classic approach based on homologous recombination (Cruz et al., 1991). With this method, we were able to replace the first *CEPT* allele with the puromycin resistance gene (*PAC*) generating *CEPT+/-* parasites (Fig. 2A). However, repeated attempts to delete the second *CEPT* allele with the blasticidin resistance gene (*BSD*) were unsuccessful, suggesting that CEPT was indispensable for promastigotes. To overcome this obstacle, we used an episome facilitated approach to acquire the chromosomal knockouts (Murta et al., 2009). Briefly, *CEPT* was cloned into the pXNG4 vector which contains genes for nourseothricin resistance (*SAT*), green fluorescent protein (GFP), and thymidine kinase (TK). The pXNG4-*CEPT* plasmid was then introduced into *CEPT+/-* to generate *CEPT+/- +*pXNG4-*CEPT*, followed by the replacement of the second chromosomal *CEPT* allele with *BSD*. With this method, parasites showing resistance to puromycin, nourseothricin, and blasticidin were readily obtained. Individual clones were isolated from these parasites by serial dilution. In a Southern blot analysis, these clones (*cept⁻* +pXNG4-*CEPT* #2-2, 2-3 and 2-4) showed a complete loss of chromosomal *CEPT* while maintaining a high level of episomal *CEPT* (Fig. 2A). No significant difference was detected among these clones and results from *cept⁻* +pXNG4-*CEPT* #2-3 were described in the following experiments. As shown in Fig. 2B, overexpression of *CEPT* had little impact on promastigote replication in culture. The fact that chromosomal null mutants could only be generated in the presence of a complementing plasmid suggests that CEPT is essential during the promastigote stage of *L. major*.

Expression and localization of CEPT in *L. major*.

The relative transcript levels of *CEPT* in wild type (WT) promastigotes (from *in vitro* culture) and amastigotes (isolated from infected BALB/c mice) were examined by qRT-PCR. Using the 28S RNA as the internal standard, we detected a three-fold reduction in *CEPT* transcript level in amastigotes in comparison to promastigotes (Fig. 3A), suggesting that this enzyme is in lower demand during the intracellular stage. In *T. brucei*, EPT and CEPT are located in different (although overlapping) sub-compartments of the endoplasmic reticulum (ER), suggesting a spatial segregation of ether lipids (e.g. PME) and diacyl-PE/PC synthesis (Farine et al., 2015). To determine the cellular localization of CEPT in *L. major*, GFP-*CEPT* was introduced into WT promastigotes (Fig. S1). In immunofluorescence microscopy, GFP-*CEPT* exhibited a diffused and membranous pattern resembling that of the ER marker BiP (Fig. 3B-F). Quantitative analysis revealed ~73% overlap between GFP-*CEPT* and BiP (Table S1), suggesting that CEPT is primarily located at the bulk ER. This is similar to the localization of EPT and CPCT in *L. major* (Pawlowic et al., 2016; Moitra et al., 2019).

CEPT is responsible for PC synthesis from CDP-choline and DAG

To determine whether *L. major* CEPT catalyzes the synthesis of PC, promastigote lysates were incubated with [^{14}C]-CDP-choline and DAG for 1 hour followed by lipid extraction and

9

339 thin layer chromatography (TLC). As illustrated in Fig. 4, overexpression of *CEPT* or *GFP-*
340 *CEPT* led to robust production of [^{14}C]-PC in the organic fraction. CEPT activity was also
341 present in the mouse liver lysate (positive control). In comparison, this activity was barely
342 detectable in WT parasites and completely absent in heat-inactivated lysates. Hydrolysis of CDP-
343 choline into choline was also detected from unboiled samples. As expected, the majority of
344 [^{14}C]-CDP-choline (a substrate) was found in the aqueous phase (Fig. 4). These findings suggest
345 that CEPT is a functional enzyme capable of generating PC from CDP-choline and DAG in *L.*
346 *major*. We were unable to confirm the contribution of CEPT to PE synthesis due to the lack of
347 commercially available, radiolabeled CDP-EtN.
348
349 **CEPT is indispensable for *L. major* promastigotes.**
350   To critically evaluate whether CEPT is required for *L. major* promastigotes, ganciclovir
351 (GCV) was added to *CEPT*+/− +pXNG4-*CEPT* and *cept⁻* +pXNG4-*CEPT* parasites which
352 would trigger the formation of GCV-triphosphate through the activity of TK, resulting in
353 premature termination of DNA synthesis. If the episomal copy of CEPT in pXNG4-*CEPT* is
354 dispensable, it would be gradually lost during *in vitro* culture in the presence of GCV (Murta et
355 al., 2009). This process was monitored by flow cytometry (the pXNG4 plasmid contains GFP)
356 and qPCR over multiple passages in culture (Fig. 5). As expected, when cultivated in the
357 presence of nourseothricin (SAT) and absence of GCV, 90-95% of *CEPT*+/− +pXNG4-*CEPT*
358 and *cept⁻* +pXNG4-*CEPT* promastigotes showed high GFP expression by flow cytometry (Fig.
359 5A). When cultivated in the absence of GCV or nourseothricin, the *CEPT*+/−+pXNG4-*CEPT*
360 parasites gradually lost the episome from 92% GFP-high in passage 1 to <4 % in passage 10
361 (Fig. 5A). In the presence of GCV and absence of nourseothricin, the reduction of GFP
362 fluorescence was much faster in these parasites (<1% GFP-high by passage 5, Fig. 5A).
363 Meanwhile, the *cept⁻* +pXNG4-*CEPT* parasites were 40-50% GFP-high after 10 passages in the
364 absence of GCV (Fig. 5A). Importantly, continuous GCV treatment did not significantly reduce
365 the GFP-high percentage in these cells (Fig. 5A-D). Thus, unlike the *CEPT*+/−+pXNG4-*CEPT*
366 parasites which had a chromosomal *CEPT* allele, *cept⁻* +pXNG4-*CEPT* parasites could not fully
367 lose the episome even when they were under strong negative selection pressure.
368
369   Next, we examined if it was possible to isolate viable and replicative *CEPT*-null
370 promastigotes without the episome. First, *cept⁻*+pXNG4-*CEPT* parasites were continuously
371 cultivated in the presence of GCV and absence of nourseothricin for 16 passages. As shown in
372 Fig. 5D, ~53% of these cells were classified as GFP-low and ~47% were classified as GFP-high.
373 We then separated the GFP-low and GFP-high populations by fluorescence-activated cell sorting
374 (FACS), followed by serial dilution to isolate clones from these populations. Importantly, when
375 these GFP-low clones were cultivated in drug-free M199 media, 31-35% of them were GFP-high
376 (Fig. 5E-F). Furthermore, qPCR analyses revealed averages of 1.64 copies of pXNG4-*CEPT*
377 plasmid per cell in the sorted GFP-low clones and 4.36 copies per cell in the sorted GFP-high
378 clones (Fig. 5G). Meanwhile, the pre-sorting population in Fig. 5D (*cept⁻*+pXNG4-*CEPT* grown
379 in GCV for 16 passages) had 2.42 copies/cell (Fig. 5G). As a control, *cept⁻*+pXNG4-*CEPT*
380 promastigotes cultured in the presence of nourseothricin retained 24.12 copies/cell (Fig. 5G).
381 Together, these results indicate that CEPT is essential for cell survival and proliferation during
382 the promastigote stage of *L. major*.
383
384 **CEPT is dispensable for *L. major* amastigotes.**

385   To investigate whether CEPT is required during the amastigote stage, we infected
386 BALB/c mice in the footpad with WT, *CEPT+/- +pXNG4-CEPT* or *cept⁻+pXNG4-CEPT*
387 promastigotes. Half of the infected mice received daily treatment of GCV for 14 days and the
388 other half received equivalent amount of sterile PBS as controls. Parasite virulence was assessed
389 by measuring the development of footpad lesions and parasite growth in mice was determined by
390 limiting dilution assay (LDA) and qPCR analysis. No significant difference in body weight was
391 detected between GCV and PBS treated mice (Fig. S2). As expected, mice infected by WT
392 parasites were not affected by GCV treatment in footpad lesion development (Fig. 6A). Similar
393 results were observed in mice infected by *CEPT+/- +pXNG4-CEPT* and *cept⁻+pXNG4-CEPT*
394 parasites as no significant differences were detected between the GCV- and PBS-treated groups
395 (Fig. 6A). We then determined parasite numbers in the footpads of infected mice at 6-, 8- and 9-
396 weeks post infection (Fig. 6B-C). While all groups showed robust parasite loads which increased
397 over time, mice infected by *cept⁻+pXNG4-CEPT* (both GCV- and PBS-treated groups) had
398 more parasites than other groups at 6- and 8-weeks post infection (Fig 6B-C, 9-week data were
399 not available for *cept⁻+pXNG4-CEPT* because those mice had reached the humane endpoint
400 after 8 weeks). These results were largely in agreement with the lesion development displayed by
401 infected mice (Fig. 6A). Thus, *cept⁻+pXNG4-CEPT* parasites are fully virulent and proliferative
402 in BALB/c mice even after GCV treatment.
403
404   Next, we examined whether *CEPT+/- +pXNG4-CEPT* and *cept⁻+pXNG4-CEPT*
405 parasites would retain the pXNG4-*CEPT* plasmid in mice. To do so, qPCR analyses were
406 performed on the amastigote DNA isolated from infected mice at 6-, 8-, and 9-weeks post
407 infection using primers for the pXNG4 plasmid (to determine plasmid copy number) and for the
408 *L. major* 28S rRNA gene (to determine parasite number). The average plasmid copy number per
409 cell was determined by dividing the total number of pXNG4 plasmid molecules with the total
410 number of parasites. As illustrated in Fig. 6D, *CEPT+/- +pXNG4-CEPT* amastigotes contained
411 0.08-0.18 copies of the episome per cell in PBS-treated mice at weeks 6-8 post infection, and
412 GCV-treatment further reduced the average copy number to 0.01-0.03 per cell. At week 9 post
413 infection, the pXNG4 copy number became nearly undetectable (<0.01, Fig. 6D). Importantly,
414 similar results were obtained for the *cept⁻+pXNG4-CEPT* amastigotes as the episome copy
415 numbers were 0.10−0.40 copies per cell in PBS-treated mice and 0.01−0.07 copies per cell in
416 GCV-treated mice (Fig. 6D). As controls, promastigotes of *CEPT+/- +pXNG4-CEPT* and
417 *cept⁻/+pXNG4-CEPT* cultivated in the presence of nourseothricin contained 19-24 copies of
418 pXNG4-*CEPT* per cell, and those cultured in the presence of GCV contained 1.6-4.4 copies per
419 cell (Fig. 6D and Fig. 5G). The fact that *cept⁻+pXNG4-CEPT* amastigotes were fully virulent
420 and replicative with very few copies of the episome (much less than one plasmid per cell)
421 suggests that CEPT is dispensable during the mammalian (intracellular) phase. These findings
422 are distinct from our previously reported *fpps⁻+pXNG4-FPPS* parasites (Mukherjee et al.,
423 2019). Thus, the *de novo* synthesis of PC is only required for the promastigote but not amastigote
424 stage in *L major*.
425
426   Our conclusion was also supported by comparing the parasite loads data from LDA and
427 qPCR (Fig. 6B-C). For WT and *CEPT+/- +pXNG4-CEPT* parasites, results from LDA and
428 qPCR were largely comparable (Fig. 6B-C). In contrast, for *cept⁻+pXNG4-CEPT*, the qPCR
429 results were 4-10 times higher than the corresponding LDA results (2-6 x 10^7 vs 2-20 x 10^6, Fig.
430 6C). While qPCR revealed the total number of amastigotes in the infected footpad, LDA only

11

431 detected those promastigotes that had successfully converted from amastigotes and replicated *in*
432 *vitro*. It appears that only a fraction of *cept⁻*+pXNG4-*CEPT* amastigotes can be converted into
433 proliferative promastigotes due to their low episome copy number (more on this point below).
434
435 **Cept⁻+pXNG4-*CEPT* parasites regain the plasmid after conversion from amastigotes to**
436 **promastigotes**
437   The apparent lack of episome in *cept⁻*+pXNG4-*CEPT* amastigotes (Fig. 6D) prompted
438 us to examine their ability to convert to promastigotes and proliferate in culture in more detail.
439 First, *CEPT*+/- +pXNG4-*CEPT* and *cept⁻*+pXNG4-*CEPT* amastigotes were isolated from
440 infected mice (Fig. 6) and allowed to recover in complete M199 media in the absence or
441 presence of nourseothricin ("no drug" or "+ SAT" in Fig. 7A). After amastigotes had converted
442 into promastigotes (in 2-4 days), they were cultivated in the absence or presence of
443 nourseothricin for 10 consecutive passages and their GFP fluorescence levels were determined
444 by flow cytometry (Fig. 7B-E). Without the positive selection drug nourseothricin,
445 *cept⁻*+pXNG4-*CEPT* parasites isolated from PBS-treated mice showed 40-60% GFP-high cells,
446 whereas *CEPT*+/- +pXNG4-*CEPT* parasites lost most of the GFP-high cells (Fig. 7B). Very
447 similar results were observed for the parasites isolated from GCV-treated mice except that the
448 GFP-high population in *cept⁻*+pXNG4-*CEPT* was ~15% in the first passage before going up to
449 50-60% in the later passages (Fig. 7C). The slower recovery may be due to the extremely low
450 episome copy number in parasites isolated from in GCV-treated mice (0.01-0.07/cell for
451 *cept⁻*+pXNG4-*CEPT*, Fig. 6D).
452
453   Meanwhile, if parasites were continuously cultivated in the presence of nourseothricin,
454 both *cept⁻*+pXNG4-*CEPT* and *CEPT*+/- +pXNG4-*CEPT* exhibited 80-90% GFP-high cells if
455 they were isolated from PBS-treated mice (Fig. 7D). However, parasites isolated from GCV-
456 treated mice failed to grow in the presence of nourseothricin (Fig. 7E). These results suggest that
457 the extremely low episome levels in *CEPT*+/- +pXNG4-*CEPT* and *cept⁻*+pXNG4-*CEPT*
458 amastigotes isolated from GCV-treated mice (0.01−0.07 copies per cell, Fig. 6D) prevented these
459 parasites from converting into proliferative promastigotes in the presence of nourseothricin.
460
461   In addition, the effect of GCV on promastigote proliferation was examined (Fig. S3). If
462 *cept⁻*+pXNG4-*CEPT* amastigotes were allowed to convert into promastigotes in the absence of
463 GCV ("no drug" in Fig. S3A), no significant difference in replication was observed (Fig. S3B).
464 This was consistent with the rapid restoration of episome level in *cept⁻*+pXNG4-*CEPT* (Fig. 7).
465 However, if these amastigotes were forced to convert into promastigotes in the presence of GCV
466 ("+ GCV" in Fig. S3A), they showed a 24-96 hours delay during the first passage ("P1" in Fig.
467 S3B). This delay was likely caused by the difficulty of these cells trying to increase their
468 episome copy numbers to support growth while balancing the toxic effect from GCV. They were
469 able to proliferate normally after the first passage ("P2-P4" in Fig. S3B), suggesting adaptation
470 to limiting the pXNG4 copy number to proper levels that satisfy the need of PC synthesis while
471 limiting toxicity. We also analyzed the pXNG4-*CEPT* DNA from those recovered culture
472 promastigotes (Fig. 7 and Fig. S3) and did not detect any mutations in the plasmid based on
473 restriction enzyme digestion and sequencing.
474
475   These findings suggest that when *cept⁻*+pXNG4-*CEPT* amastigotes were allowed to
476 recover during the initial passage in culture, they quickly elevated the plasmid copy numbers

12

477   while transitioning to promastigotes. This occurred even in the absence of nourseothricin (the
478   selection drug for pXNG4 plasmid) and presence of GCV due to the essentiality of CEPT in
479   promastigotes. In contrast, for *CEPT*+/- +pXNG4-*CEPT*, the plasmid copy number did not
480   increase without strong positive selection.
481
482   **Cept‾+pXNG4-*CEPT* parasites showed similar PC and PE contents as WT parasites**
483   Next, we determined the lipid composition in *cept‾*+pXNG4-*CEPT* parasites to evaluate
484   the impact of CEPT on PC/PE production. First, total lipids from culture promastigotes were
485   examined by ESI-MS in the positive ion mode to detect PC (as protonated $[M+H]^+$ ions) and
486   negative ion mode to detect PE (as deprotonated $[M-H]^-$ ions). As indicated in Fig. S4A, the
487   majority of PC in promastigotes were 1,2-diacyl types with polyunsaturated FAs at the sn-2
488   positions (e.g., 18:2/22:6 PC, 18:3/22:6 PC and 16:1/20:4 PC) while ether PC (e.g., a18:0/20:2
489   PC and e18:1/24:6 PC) were less common. These findings were largely in agreement with
490   previous reports (Weingartner et al., 2012; Williams et al., 2012). No statistically significant
491   difference in PC composition was detected between WT and *cept‾*+pXNG4-*CEPT*
492   promastigotes (Fig. S4A). Similarly, the composition for PE (mainly e18:0/18:2 PE and
493   e18:0/18:1 PE, both are PME) in *cept‾*+pXNG4-*CEPT* were very similar to WT promastigotes
494   (Fig. S4B) (Zhang et al., 2007).
495
496   Finally, we examined the lipids from lesion-derived amastigotes (Fig. S5) and uninfected
497   mouse footpads. As summarized in Fig. 8A, the PC in WT amastigotes included both ether lipids
498   (e.g., a16:0/16:0 PC, a16:0/18:2 PC, and a16:0/18:1 PC) and 1,2-diacyl types (e.g., 36:4 PC, 36:2
499   PC and 34:2 PC). Importantly, very similar PC composition was found in *cept‾*+pXNG4-*CEPT*
500   amastigotes despite the near complete loss of *CEPT* gene in these parasites (Fig. 8A and 6D).
501   Thus, *L. major* amastigotes can acquire the majority of their PC in the absence of *de novo*
502   synthesis. While some of these amastigote PC (e.g., 36:4 PC, 34:2 PC and 34:1 PC) were also
503   found in uninfected mouse tissue, the majority of amastigote PC were of low abundance or
504   undetectable in the host (Fig. 8A) (e.g., a16:0/16:0 PC, a16:0/18:2 PC and a16:0/18:1 PC). These
505   findings suggest that amastigotes can generate PC through the uptake and remodeling of host PC.
506
507   In comparison to PC, we found higher degrees of overlap in the composition of
508   triacylglycerol (TAG) and PE between amastigotes and mouse tissue (Fig. 8B and C). Again, no
509   major differences in TAG and PE composition were detected between WT and *cept‾*+pXNG4-
510   *CEPT* amastigotes (Fig. 8B and C). In summary, our data indicate that the *de novo* PC synthesis
511   is dispensable for the survival and proliferation of intracellular amastigotes which can salvage
512   and remodel lipids from the host.
513

DISCUSSION

514
515
516   *Leishmania* parasites can synthesize PC from multiple routes including the choline
517   branch of the Kennedy pathway, the N-methylation of PE and the salvage/remodeling of host
518   lipids (Fig. 1). In this study, we characterized the gene encoding CEPT in *L. major* which
519   catalyzes the formation of PC from CDP-choline and DAG, the final step of *de novo* PC
520   synthesis (Fig. 1 and 4). Similar to CPCT and EPT, CEPT is primarily located at the ER (Fig. 3)
521   (Pawlowic et al., 2016; Moitra et al., 2019). While both the choline branch and ethanolamine
522   branch are essential for survival in *T. brucei* (Gibellini et al., 2009; Gibellini and Smith, 2010),
523   *Leishmania* parasites can tolerate the loss of several Kennedy pathway enzymes presumably
524   from the compensatory effects of other pathways, as evidenced by the *cpct⁻* and *ept⁻* mutants
525   (Pawlowic et al., 2016; Moitra et al., 2019). However, we could not generate the chromosomal
526   *CEPT* null mutant in culture without first introducing a complementing episome (Fig. 2).
527   Attempts to eliminate the GFP-containing pXNG4-*CEPT* episome via prolonged GCV-treatment
528   in culture were unsuccessful in *cept⁻*+pXNG4-*CEPT*, as 40-50% of parasites remained GFP-
529   high (Fig. 5A). Even after cell sorting and serial dilution, clones derived from the GFP-low
530   population still displayed 31-35% GFP-high with 1.5-2 copies of pXNG4-*CEPT* episome per cell
531   (Fig. 5D-G). Thus, those GFP-low *cept⁻*+pXNG4-*CEPT* parasites likely contained the pXNG4-
532   *CEPT* episome at a low but detectable level or they could not proliferate without the GFP-high
533   cells. Interestingly, *Leishmania* and *T. brucei* parasites are known to produce and exchange
534   extracellular vesicles among individual cells (Douanne et al., 2020). Such transfer of cellular
535   material may contribute to the survival of *cept⁻*+pXNG4-*CEPT* parasites after GCV treatment.
536
537   Because CEPT is also expected to catalyze the synthesis of diacyl-PE, its deletion would
538   not only block the choline branch of the Kennedy pathway, but also reduce PC synthesis from
539   PE N-methylation (Fig. 1). Therefore, while *L. major* promastigotes can withstand the deletion
540   of CPCT, a complete loss of CEPT would drastically compromise their ability to generate PC.
541   The essentiality of *CEPT* in promastigotes suggests that the salvage pathway by itself cannot
542   produce enough PC (the most abundant lipids) to support parasite proliferation in culture.
543
544   In contrast to the promastigote stage, CEPT appears to be dispensable during the
545   intracellular amastigote stage. In mice infected by *cept⁻*+pXNG4-*CEPT* parasites, GCV
546   treatment was able to dramatically reduce the episome level to 0.01-0.07 copy per cell after 6-8
547   weeks (Fig. 6D). While this analysis was done at the DNA level, it suggests that the majority of
548   *cept⁻*+pXNG4-*CEPT* amastigotes lack CEPT mRNA and protein. Nonetheless, these
549   chromosomal-null mutants were fully virulent and replicative in mice (Fig. 6A-C). In fact, these
550   *cept⁻*+pXNG4-*CEPT* parasites showed slightly better growth than WT parasites in mice,
551   suggesting that they gained a small advantage by losing *de novo* PC synthesis (Fig. 6B-C).
552   Additionally, lipidomic analysis revealed very similar PC contents between WT and
553   *cept⁻*+pXNG4-*CEPT* amastigotes (Fig. 8A). The total PC levels in WT and *cept⁻*+pXNG4-
554   *CEPT* amastigotes also appeared to be similar based on the signal intensity from mass
555   spectrometry. Thus, *L. major* amastigotes are capable of generating sufficient amounts of PC in
556   the absence of *de novo* synthesis. This is consistent with the three-fold reduction of *CEPT*
557   transcript level when parasites transition from promastigotes to amastigotes (Fig. 3A).
558

559   In theory, amastigotes could acquire PC from the mammalian host, either by directly
560   incorporating host lipids or converting them into their own. As indicated in Fig. 8A, while
561   certain PC types were present in both amastigotes and mice, the majority of amastigote PC
562   including the most abundant species like a16:0/16:0 PC and a16:0/18:2 PC were of low
563   abundance or undetectable in uninfected mouse tissue, suggesting that they were modified from
564   host lipids. The mechanism by which amastigotes remodel host lipids is under investigation. In
565   many eukaryotes, phospholipase A2 (PLA2) removes fatty acids at the sn-2 position of PC, and
566   the resulting lysophosphatidylcholine can be re-acylated at the sn-2 position to yield a different
567   PC (Lands cycle)(Lands, 1958). Genes encoding PLA2 and lysophosphatidylcholine
568   acyltransferase are present in *Leishmania* genomes suggesting that they can carry out lipid
569   remodeling via deacylation/re-acylation. The Lands cycle is also present in the intestinal
570   protozoan *Giardia lamblia* which has a limited capacity for *de novo* lipid synthesis (Das et al.,
571   2001). In addition to PC remodeling and *de novo* synthesis, it is also possible for amastigotes to
572   generate PC through the N-methylation of salvaged PE (Fig. 1).
573
574   Comparing to PC, higher degrees of overlap were observed in the compositions of
575   triacylglycerol (TAG) and PE between amastigotes and uninfected mouse tissue (Fig. 8B-C).
576   These findings support the direct incorporation of these lipids by amastigotes similar to the
577   reported uptake of host TAG by intracellular *T. cruzi* parasites (Gazos-Lopes et al., 2017),
578   although further investigation is warranted. Overall, the ability of *Leishmania* amastigotes to take
579   up and remodel host PC is in agreement with their propensity to incorporate host sphingolipids
580   and cholesterol (Zhang et al., 2005; Xu et al., 2014). Since *Leishmania* amastigotes spend the
581   majority of their time in mammals in a slow growing, quiescent state (estimated doubling time:
582   60 hours) (Saunders et al., 2014; Mandell and Beverley, 2017), the salvage pathway (which is
583   less energy intensive than *de novo* synthesis) seems to fit the intracellular stage. In contrast, the
584   *de novo* synthesis is required to generate sufficient amount of lipids to support parasite
585   replication during the promastigote stage (doubling time: 6-8 hours). The ability of *Leishmania*
586   parasites to acquire sufficient lipids via either *de novo* synthesis or salvage/remodeling (the
587   metabolic flexibility) may allow them to adapt to a diverse range of host cells and host species.
588   Future studies will elucidate how amastigotes regulate the uptake and remodeling of different
589   classes of lipids and explore the potential of blocking the transfer of host lipids to parasites as a
590   novel therapeutic.

FIGURE LEGENDS

Figure 1. Acquisition of PE and PC in *Leishmania*. E/CK: ethanolamine/choline kinase; EPCT: ethanolaminephosphate cytidylyltransferase; EPT: ethanolamine phosphotransferase; CPCT: cholinephosphate cytidylyltransferase; CEPT: choline ethanolamine phosphotransferase; PEMT: phosphatidylethanolamine N-methyltransferase; PSS2: phosphatidylserine synthase 2; PSD: phosphatidylserine decarboxylase; EtN: ethanolamine; EtN-P: ethanolamine phosphate; PE: (1,2-diacyl-) phosphatidylethanolamine; PME: plasmenylethanolamine; Choline-P: choline phosphate; PC: phosphatidylcholine; PS: phosphatidylserine.

Figure 2. Deletion of *L. major CEPT* in the presence of pXNG4-*CEPT*. (**A**) Genomic DNA samples from WT, *CEPT* +/- clone #2, *CEPT* +/- +pXNG4-*CEPT* (clone #2), and *cept⁻* +pXNG4-*CEPT* (clones #2-3, 2-3, and 2-4) parasites were processed for Southern blot using radiolabeled probes for the ORF (top) or flanking sequence (bottom) of *CEPT*. Bands corresponding to chromosomal *CEPT* (top: 8252 bp, bottom: 3730 bp), pXNG4-*CEPT* (top: 3475 bp), *PAC* (bottom: 3076 bp) and *BSD* (bottom: 2876 bp) were indicated. (**B**) Promastigotes of WT, *CEPT* +/- +pXNG4-*CEPT*, and *cept⁻* +pXNG4-*CEPT* were cultivated at 27 °C in complete M199 media and culture densities were determined using a hemocytometer. Error bars represent standard deviations from three experiments.

Figure 3. Transcript level and localization of CEPT in *L. major*. (**A**) The transcript level of *CEPT* was determined from culture promastigotes and lesion-derived amastigotes by qRT-PCR. The relative abundance of *CEPT* transcript was normalized using 28S RNA as the internal control based on ΔΔCt values. Error bars represent standard deviations from two independent biological repeats. (**B**)-(**F**) Log phase promastigotes of WT+pXG-*GFP-CEPT* were labeled with rabbit *anti-T. brucei* BiP antiserum followed by a goat anti-rabbit IgG-Texas Red antibody and subjected to immunofluorescence microscopy. (**B**) Differential interference contrast; (**C**) DNA staining; (**D**) GFP fluorescence; (**E**) Anti-BiP staining; (**F**) Merge of **D** and **E**. Scale bar: 10 µm. The overlap between BiP and GFP-CEPT was determined by the JaCOP Image J analysis of 136 cells (Table S1).

Figure 4. CEPT is responsible for the synthesis of PC from CDP-choline and DAG. Mouse liver lysate or promastigote lysate were incubated with [¹⁴C]-CDP-choline and DAG followed by extraction with 1-butanol and TLC analysis as described in *Materials and Methods*. Lane 1: [¹⁴C]-CDP-choline. Lane 2: [¹⁴C]-1,2-diarachidonyl PC. Lane 3-8: Organic fractions after 1-butanol extraction. Lane 9-11: aqueous fractions after 1-butanol extraction. O: origin. F: Solvent front. This assay was repeated three times and results from one representative experiment were shown here.

Figure 5. CEPT is indispensable for *L. major* promastigotes. (**A**) Promastigotes were continuously cultivated in the presence or absence of GCV or nourseothricin (SAT) and percentages of GFP-high cells were determined by flow cytometry for each passage. (**B-D**) After 16 passages, flow cytometry analyses were performed on WT parasites (**B**), *cept⁻* +pXNG4-*CEPT* parasites grown in the presence of nourseothricin (**C**) or GCV (**D**). (**E-F**) Two clones of *cept⁻* +pXNG4-*CEPT* were isolated from the GFP-low population in **D** by serial dilution and subjected to flow cytometry. In **B-F**, percentages of GFP-high cells (summarized in **A**) were

17

644 indicated as R2. (**G**) The GFP-high and GFP–low parasites in **D** were separated by FACS, and
645 plasmid copy numbers were determined by qPCR as described in *Materials and Method*s. Error
646 bars represent standard deviations from two or three biological repeats (*: $p<0.05$, **: $p<0.01$).
647
648 **Figure 6. CEPT is dispensable for *L. major* amastigotes.** BALB/c mice were infected in the
649 footpads with stationary phase promastigotes and treated with either GCV or PBS from day 1 to
650 day 14 post infection as described in *Materials and Methods*. (**A**) Footpad lesions were recorded
651 weekly. (**B**)-(**C**) Parasite numbers in the infected footpads were determined at the indicated times
652 by limiting dilution assay (**B**) and qPCR (**C**). (**D**) The pXNG4-*CEPT* copy numbers in
653 promastigotes and amastigotes (#/cell $\pm$ SDs) were determined by qPCR. The 9 weeks data for
654 *cept⁻* +pXNG4-*CEPT* amastigotes were not available (NA) because the infected mice had
655 reached the humane endpoint at 8 weeks. Error bars represent standard deviations (*: $p < 0.05$,
656 **: $p < 0.01$, ***: $p < 0.001$).
657
658 **Figure 7. *Cept⁻*+pXNG4-*CEPT* parasites restore their episome levels after converting to**
659 **promastigotes.** (**A**) Amastigotes from infected BALB/c mice were allowed to recover in
660 complete M199 media in the absence or presence of 200 µg/ml of nourseothricin (+ SAT).
661 Promastigotes were then continuously cultivated in the absence (**B** and **C**) or presence (**D** and **E**)
662 of nourseothricin for 10 passages and percentages of GFP-high cells were analyzed by flow
663 cytometry for each passage. It is of note that no cells from GCV-treated mice were able to
664 recover in nourseothricin (**E**). For **B**-**D**, error bars represent standard deviations from two
665 independent biological experiments (two technical duplicates each time).
666
667 **Figure 8. *Cept⁻*+pXNG4-*CEPT* amastigotes show similar composition of PC and PE as WT**
668 **amastigotes.** Amastigotes were isolated from the footpad of infected BALB/c mice. Lipids from
669 partially purified amastigotes and uninfected mouse footpad tissue were analyzed by ESI-MS in
670 the positive ion mode (**A** and **B**) and negative ion mode (**C**). Compositions for PC (**A**), TAG (**B**),
671 and PE (**C**) were summarized. Only major lipid species (>20% for PC and >10% for TAG and
672 PE) by relative abundance are shown. Predicted formulas and molecular weights were indicated
673 for each lipid species (*a*: 1-alkyl phospholipids, *e*: 1-alkenyl phospholipids, lyso: 1-
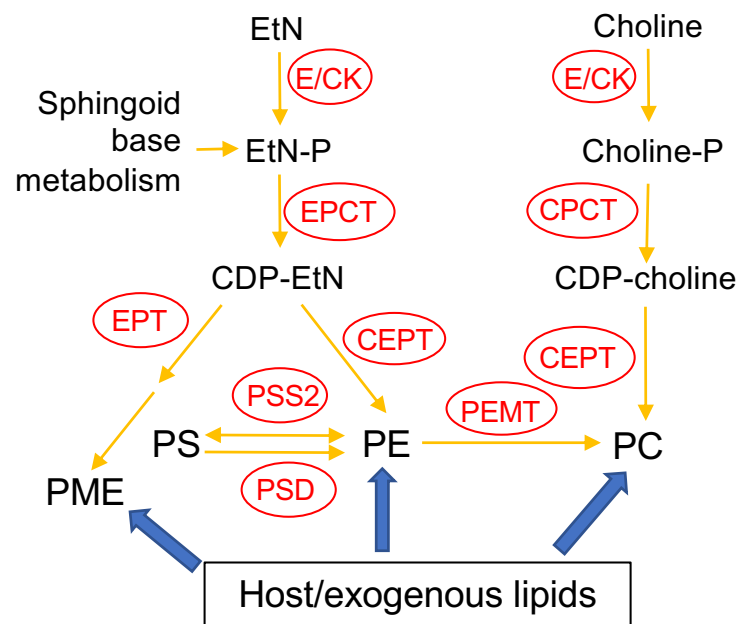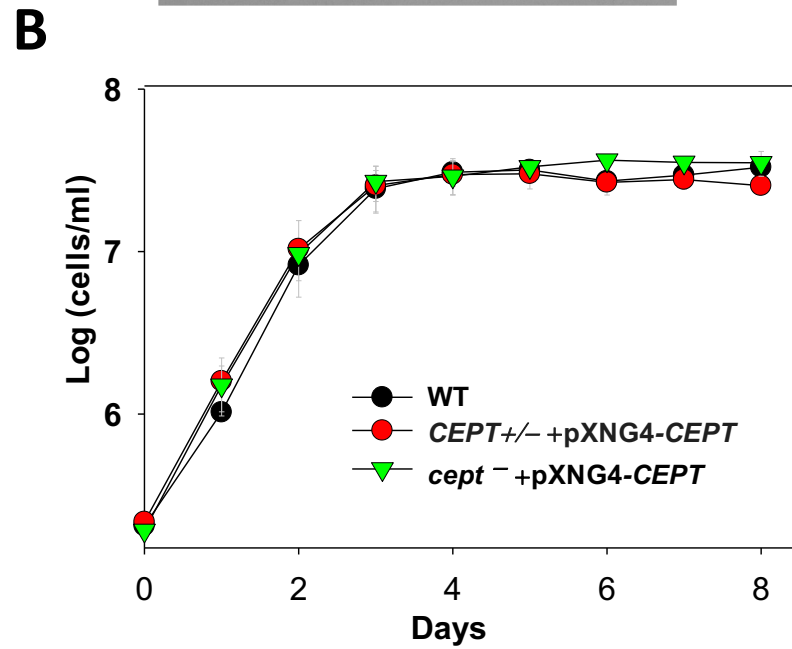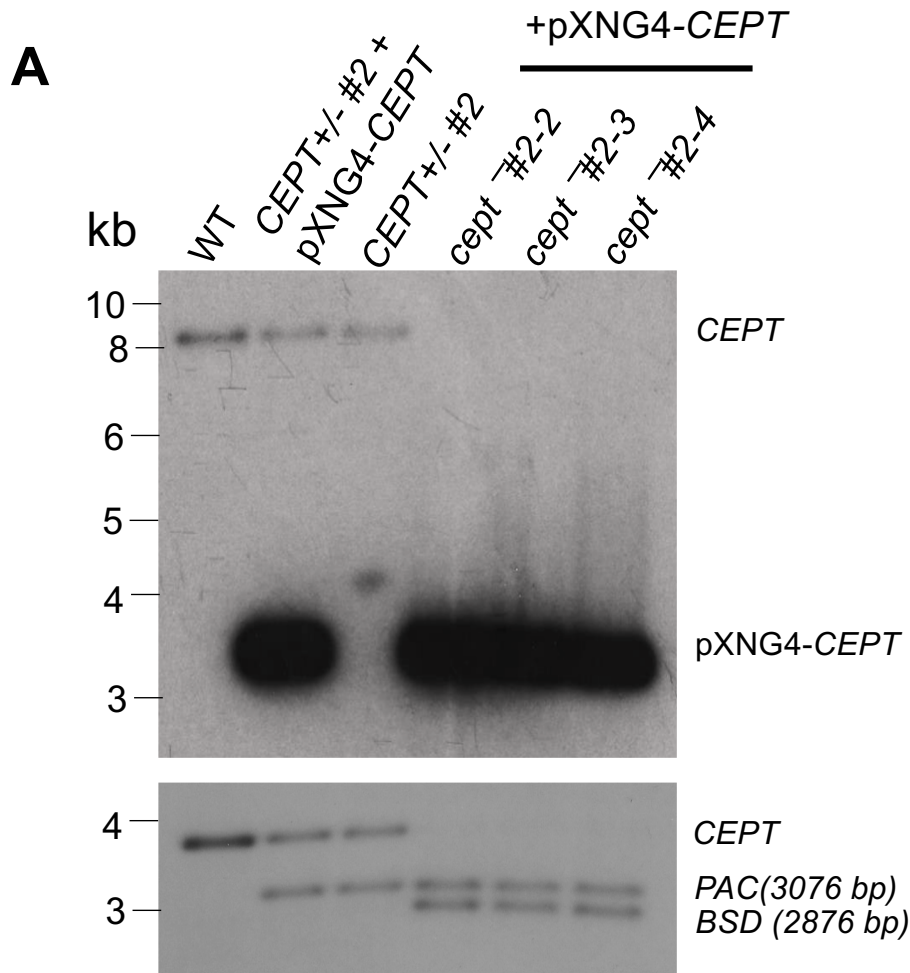674 lysophospholipids).

REFERENCES

Alvar, J., Velez, I.D., Bern, C., Herrero, M., Desjeux, P., Cano, J., et al. (2012). Leishmaniasis worldwide and global estimates of its incidence. *PLoS One* 7(5)**,** e35671. doi: 10.1371/journal.pone.0035671.

Beach, D.H., Holz, G.G., Jr., and Anekwe, G.E. (1979). Lipids of Leishmania promastigotes. *J Parasitol* 65(2)**,** 201-216.

Besteiro, S., Williams, R.A., Morrison, L.S., Coombs, G.H., and Mottram, J.C. (2006). Endosome sorting and autophagy are essential for differentiation and virulence of *Leishmania major*. *J Biol Chem* 281(16)**,** 11384-11396.

Bibis, S.S., Dahlstrom, K., Zhu, T., and Zufferey, R. (2014). Characterization of Leishmania major phosphatidylethanolamine methyltransferases LmjPEM1 and LmjPEM2 and their inhibition by choline analogs. *Mol Biochem Parasitol* 196(2)**,** 90-99. doi: 10.1016/j.molbiopara.2014.08.005.

Bligh, E.G., and Dyer, W.J. (1959). A rapid method of total lipid extraction and purification. *Can J Biochem Physiol* 37(8)**,** 911-917.

Bolte, S., and Cordelieres, F.P. (2006). A guided tour into subcellular colocalization analysis in light microscopy. *J Microsc* 224(Pt 3)**,** 213-232. doi: 10.1111/j.1365-2818.2006.01706.x.

Castanys-Munoz, E., Alder-Baerens, N., Pomorski, T., Gamarro, F., and Castanys, S. (2007). A novel ATP-binding cassette transporter from Leishmania is involved in transport of phosphatidylcholine analogues and resistance to alkyl-phospholipids. *Mol Microbiol* 64(5)**,** 1141-1153.

Croft, S.L., and Olliaro, P. (2011). Leishmaniasis chemotherapy--challenges and opportunities. *Clin Microbiol Infect* 17(10)**,** 1478-1483. doi: 10.1111/j.1469-0691.2011.03630.x.

Cruz, A., Coburn, C.M., and Beverley, S.M. (1991). Double targeted gene replacement for creating null mutants. *Proc Natl Acad Sci U S A* 88(16)**,** 7170-7174.

Cui, Z., and Vance, D.E. (1996). Expression of phosphatidylethanolamine N-methyltransferase-2 is markedly enhanced in long term choline-deficient rats. *J Biol Chem* 271(5)**,** 2839-2843.

Das, S., Castillo, C., and Stevens, T. (2001). Phospholipid remodeling/generation in Giardia: the role of the Lands cycle. *Trends Parasitol* 17(7)**,** 316-319.

Douanne, N., Dong, G., Douanne, M., Olivier, M., and Fernandez-Prada, C. (2020). Unravelling the proteomic signature of extracellular vesicles released by drug-resistant Leishmania infantum parasites. *PLoS Negl Trop Dis* 14(7)**,** e0008439. doi: 10.1371/journal.pntd.0008439.

Ellens, H., Siegel, D.P., Alford, D., Yeagle, P.L., Boni, L., Lis, L.J., et al. (1989). Membrane fusion and inverted phases. *Biochemistry* 28(9)**,** 3692-3703. doi: 10.1021/bi00435a011.

Exton, J.H. (1994). Phosphatidylcholine breakdown and signal transduction. *Biochim Biophys Acta* 1212(1)**,** 26-42.

Farine, L., Niemann, M., Schneider, A., and Butikofer, P. (2015). Phosphatidylethanolamine and phosphatidylcholine biosynthesis by the Kennedy pathway occurs at different sites in Trypanosoma brucei. *Sci Rep* 5**,** 16787. doi: 10.1038/srep16787.

Furse, S., and de Kroon, A.I. (2015). Phosphatidylcholine's functions beyond that of a membrane brick. *Mol Membr Biol* 32(4)**,** 117-119. doi: 10.3109/09687688.2015.1066894.
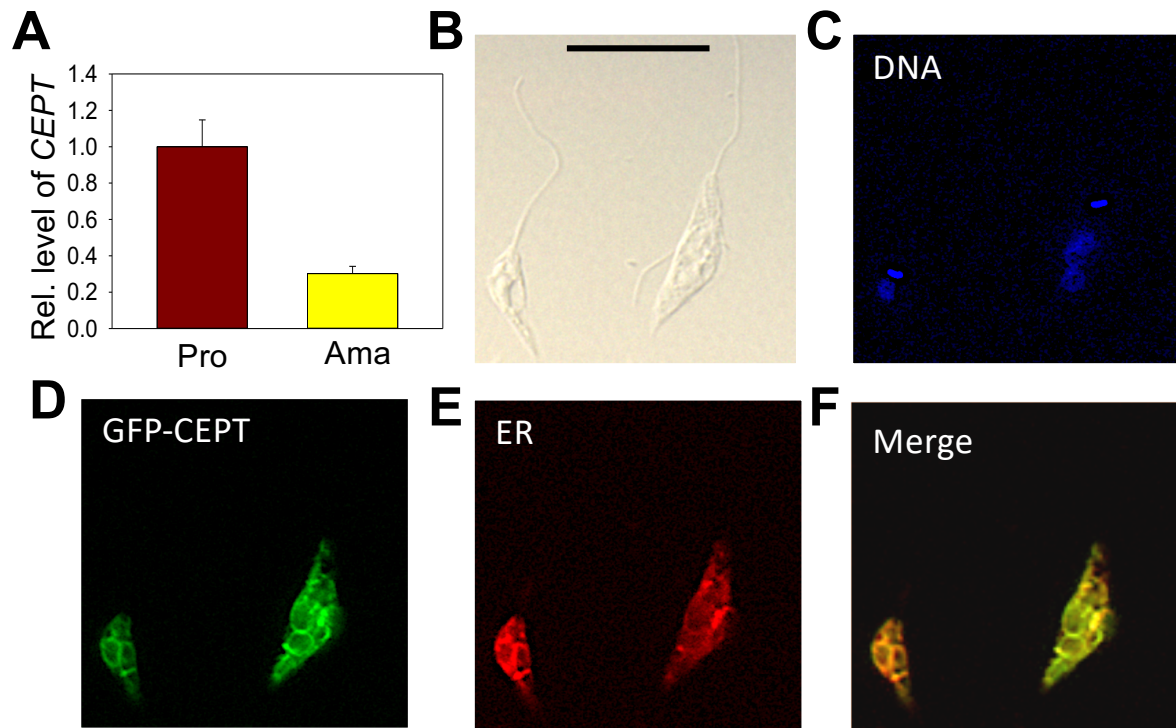
719 Gazos-Lopes, F., Martin, J.L., Dumoulin, P.C., and Burleigh, B.A. (2017). Host triacylglycerols
720   shape the lipidome of intracellular trypanosomes and modulate their growth. *PLoS*
721   *Pathog* 13(12)**,** e1006800. doi: 10.1371/journal.ppat.1006800.
722 Gibellini, F., Hunter, W.N., and Smith, T.K. (2009). The ethanolamine branch of the Kennedy
723   pathway is essential in the bloodstream form of Trypanosoma brucei. *Mol Microbiol*
724   73(5)**,** 826-843.
725 Gibellini, F., and Smith, T.K. (2010). The Kennedy pathway--De novo synthesis of
726   phosphatidylethanolamine and phosphatidylcholine. *IUBMB Life* 62(6)**,** 414-428. doi:
727   10.1002/iub.337.
728 Glaser, T.A., Wells, S.J., Spithill, T.W., Pettitt, J.M., Humphris, D.C., and Mukkada, A.J.
729   (1990). Leishmania major and L. donovani: a method for rapid purification of
730   amastigotes. *Exp Parasitol* 71(3)**,** 343-345.
731 Ha, D.S., Schwarz, J.K., Turco, S.J., and Beverley, S.M. (1996). Use of the green fluorescent
732   protein as a marker in transfected Leishmania. *Mol Biochem Parasitol* 77(1)**,** 57-64.
733 Henneberry, A.L., and McMaster, C.R. (1999). Cloning and expression of a human
734   choline/ethanolaminephosphotransferase: synthesis of phosphatidylcholine and
735   phosphatidylethanolamine. *Biochem J* 339 (Pt 2)**,** 291-298.
736 Henriques, C., Atella, G.C., Bonilha, V.L., and de Souza, W. (2003). Biochemical analysis of
737   proteins and lipids found in parasitophorous vacuoles containing Leishmania
738   amazonensis. *Parasitol Res* 89(2)**,** 123-133.
739 Hsu, F.F., Kuhlmann, F.M., Turk, J., and Beverley, S.M. (2014). Multiple-stage linear ion-trap
740   with high resolution mass spectrometry towards complete structural characterization of
741   phosphatidylethanolamines containing cyclopropane fatty acyl chain in Leishmania
742   infantum. *J Mass Spectrom* 49(3)**,** 201-209. doi: 10.1002/jms.3327.
743 Ichimura, Y., Kirisako, T., Takao, T., Satomi, Y., Shimonishi, Y., Ishihara, N., et al. (2000). A
744   ubiquitin-like system mediates protein lipidation. *Nature* 408(6811)**,** 488-492.
745 Kapler, G.M., Coburn, C.M., and Beverley, S.M. (1990). Stable transfection of the human
746   parasite *Leishmania major* delineates a 30-kilobase region sufficient for
747   extrachromosomal replication and expression. *Mol Cell Biol* 10(3)**,** 1084-1094.
748 Kennedy, E.P. (1956). The synthesis of cytidine diphosphate choline, cytidine diphosphate
749   ethanolamine, and related compounds. *J Biol Chem* 222(1)**,** 185-191.
750 Lands, W.E. (1958). Metabolism of glycerolipides; a comparison of lecithin and triglyceride
751   synthesis. *J Biol Chem* 231(2)**,** 883-888.
752 Livak, K.J., and Schmittgen, T.D. (2001). Analysis of relative gene expression data using real-
753   time quantitative PCR and the 2(-Delta Delta C(T)) Method. *Methods* 25(4)**,** 402-408.
754 Mandell, M.A., and Beverley, S.M. (2017). Continual renewal and replication of persistent
755   Leishmania major parasites in concomitantly immune hosts. *Proc Natl Acad Sci U S A*
756   114(5)**,** E801-E810. doi: 10.1073/pnas.1619265114.
757 Menon, A.K., Eppinger, M., Mayor, S., and Schwarz, R.T. (1993). Phosphatidylethanolamine is
758   the donor of the terminal phosphoethanolamine group in trypanosome
759   glycosylphosphatidylinositols. *EMBO J* 12(5)**,** 1907-1914.
760 Moitra, S., Pawlowic, M.C., Hsu, F.F., and Zhang, K. (2019). Phosphatidylcholine synthesis
761   through cholinephosphate cytidylyltransferase is dispensable in Leishmania major. *Sci*
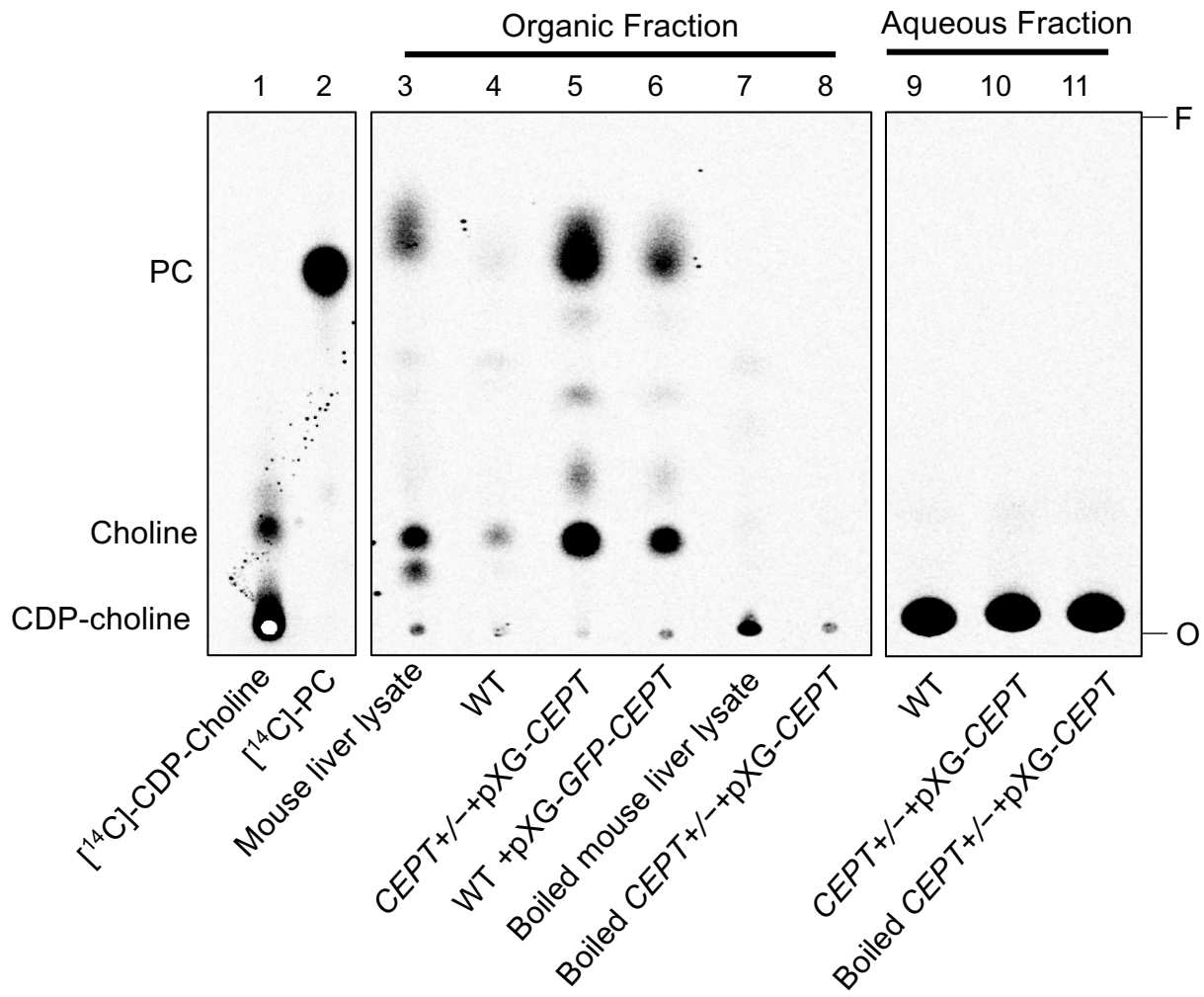762   *Rep* 9(1)**,** 7602. doi: 10.1038/s41598-019-44086-6.

763 Mukherjee, S., Basu, S., and Zhang, K. (2019). Farnesyl pyrophosphate synthase is essential for
764   the promastigote and amastigote stages in Leishmania major. *Mol Biochem Parasitol*
765   230**,** 8-15. doi: 10.1016/j.molbiopara.2019.03.001.
766 Murta, S.M., Vickers, T.J., Scott, D.A., and Beverley, S.M. (2009). Methylene tetrahydrofolate
767   dehydrogenase/cyclohydrolase and the synthesis of 10-CHO-THF are essential in
768   Leishmania major. *Mol Microbiol* 71(6)**,** 1386-1401.
769 Nickels, J.D., Smith, J.C., and Cheng, X. (2015). Lateral organization, bilayer asymmetry, and
770   inter-leaflet coupling of biological membranes. *Chem Phys Lipids* 192**,** 87-99. doi:
771   10.1016/j.chemphyslip.2015.07.012.
772 Parodi-Talice, A., Araujo, J.M., Torres, C., Perez-Victoria, J.M., Gamarro, F., and Castanys, S.
773   (2003). The overexpression of a new ABC transporter in Leishmania is related to
774   phospholipid trafficking and reduced infectivity. *Biochim Biophys Acta* 1612(2)**,** 195-
775   207.
776 Pawlowic, M.C., Hsu, F.F., Moitra, S., Biyani, N., and Zhang, K. (2016).
777   Plasmenylethanolamine synthesis in Leishmania major. *Mol Microbiol* 101(2)**,** 238-249.
778   doi: 10.1111/mmi.13387.
779 Pawlowic, M.C., and Zhang, K. (2012). Leishmania parasites possess a platelet-activating factor
780   acetylhydrolase important for virulence. *Mol Biochem Parasitol* 186(1)**,** 11-20. doi:
781   10.1016/j.molbiopara.2012.08.005.
782 Saunders, E.C., Ng, W.W., Kloehn, J., Chambers, J.M., Ng, M., and McConville, M.J. (2014).
783   Induction of a stringent metabolic response in intracellular stages of Leishmania
784   mexicana leads to increased dependence on mitochondrial metabolism. *PLoS Pathog*
785   10(1)**,** e1003888. doi: 10.1371/journal.ppat.1003888.
786 Signorell, A., Gluenz, E., Rettig, J., Schneider, A., Shaw, M.K., Gull, K., et al. (2009).
787   Perturbation of phosphatidylethanolamine synthesis affects mitochondrial morphology
788   and cell-cycle progression in procyclic-form Trypanosoma brucei. *Mol Microbiol* 72(4)**,**
789   1068-1079.
790 Signorell, A., Jelk, J., Rauch, M., and Butikofer, P. (2008a). Phosphatidylethanolamine is the
791   precursor of the ethanolamine phosphoglycerol moiety bound to eukaryotic elongation
792   factor 1A. *J Biol Chem* 283(29)**,** 20320-20329.
793 Signorell, A., Rauch, M., Jelk, J., Ferguson, M.A., and Butikofer, P. (2008b).
794   Phosphatidylethanolamine in Trypanosoma brucei is organized in two separate pools and
795   is synthesized exclusively by the Kennedy pathway. *J Biol Chem* 283(35)**,** 23636-23644.
796 Smith, T.K., and Butikofer, P. (2010). Lipid metabolism in Trypanosoma brucei. *Mol Biochem*
797   *Parasitol* 172(2)**,** 66-79.
798 Titus, R.G., Marchand, M., Boon, T., and Louis, J. (1985). A limiting dilution assay for
799   quantifying Leishmania major in tissues of infected mice. *Parasite Immunol* 7(5)**,** 545-
800   555.
801 van Meer, G., Voelker, D.R., and Feigenson, G.W. (2008). Membrane lipids: where they are and
802   how they behave. *Nat Rev Mol Cell Biol* 9(2)**,** 112-124. doi: 10.1038/nrm2330.
803 Vance, J.E. (2008). Phosphatidylserine and phosphatidylethanolamine in mammalian cells: two
804   metabolically related aminophospholipids. *J Lipid Res* 49(7)**,** 1377-1387.
805 Verkleij, A.J., Leunissen-Bijvelt, J., de Kruijff, B., Hope, M., and Cullis, P.R. (1984). Non-
806   bilayer structures in membrane fusion. *Ciba Found Symp* 103**,** 45-59. doi:
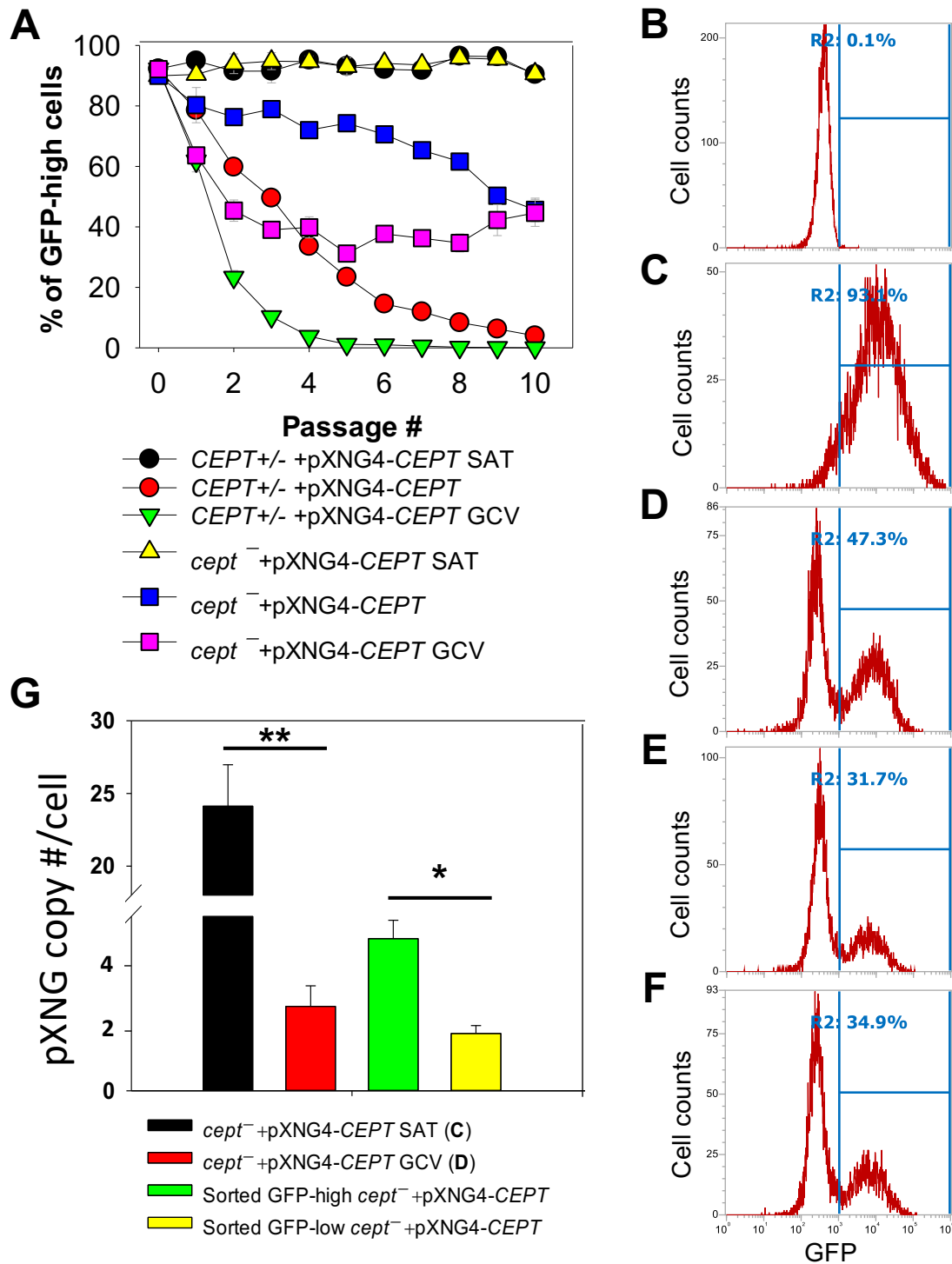807   10.1002/9780470720844.ch4.

808 Weingartner, A., Kemmer, G., Muller, F.D., Zampieri, R.A., Gonzaga dos Santos, M., Schiller,
809   J., et al. (2012). Leishmania promastigotes lack phosphatidylserine but bind annexin V
810   upon permeabilization or miltefosine treatment. *PLoS One* 7(8)**,** e42070. doi:
811   10.1371/journal.pone.0042070.
812 Williams, R.A., Smith, T.K., Cull, B., Mottram, J.C., and Coombs, G.H. (2012). ATG5 is
813   essential for ATG8-dependent autophagy and mitochondrial homeostasis in Leishmania
814   major. *PLoS Pathog* 8(5)**,** e1002695. doi: 10.1371/journal.ppat.1002695.
815 Xu, W., Hsu, F.F., Baykal, E., Huang, J., and Zhang, K. (2014). Sterol Biosynthesis Is Required
816   for Heat Resistance but Not Extracellular Survival in Leishmania. *PLoS Pathog* 10(10)**,**
817   e1004427. doi: 10.1371/journal.ppat.1004427.
818 Zachowski, A. (1993). Phospholipids in animal eukaryotic membranes: transverse asymmetry
819   and movement. *Biochem J* 294 (Pt 1)**,** 1-14. doi: 10.1042/bj2940001.
820 Zhang, K., and Beverley, S.M. (2010). Phospholipid and sphingolipid metabolism in
821   Leishmania. *Mol Biochem Parasitol* 170(2)**,** 55-64. PMCID: 2815228.
822 Zhang, K., Hsu, F.F., Scott, D.A., Docampo, R., Turk, J., and Beverley, S.M. (2005). *Leishmania*
823   salvage and remodelling of host sphingolipids in amastigote survival and acidocalcisome
824   biogenesis. *Mol Microbiol* 55(5)**,** 1566-1578.
825 Zhang, K., Pompey, J.M., Hsu, F.F., Key, P., Bandhuvula, P., Saba, J.D., et al. (2007).
826   Redirection of sphingolipid metabolism toward *de novo* synthesis of ethanolamine in
827   *Leishmania*. *EMBO J* 26(4)**,** 1094-1104.
828 Zhang, O., Xu, W., Pillai, A., Zhang, K. (2012). Developmentally Regulated Sphingolipid
829   Degradation in *Leishmania major*. *PLoS One* 7(1):e31059.
830 Zheng, L., T'Kind, R., Decuypere, S., von Freyend, S.J., Coombs, G.H., and Watson, D.G.
831   (2010). Profiling of lipids in Leishmania donovani using hydrophilic interaction
832   chromatography in combination with Fourier transform mass spectrometry. *Rapid*
833   *Commun Mass Spectrom* 24(14)**,** 2074-2082.
834 Zufferey, R., Allen, S., Barron, T., Sullivan, D.R., Denny, P.W., Almeida, I.C., et al. (2003).
835   Ether phospholipids and glycosylinositolphospholipids are not required for amastigote
836   virulence or for inhibition of macrophage activation by *Leishmania major*. *J Biol Chem*
837   278(45)**,** 44708-44718.

838

A

% of GFP-high cells vs Passage #

- *CEPT+/-* +pXNG4-*CEPT* SAT (black circle)
- *CEPT+/-* +pXNG4-*CEPT* (red circle)
- *CEPT+/-* +pXNG4-*CEPT* GCV (green triangle)
- *cept⁻* +pXNG4-*CEPT* SAT (yellow triangle)
- *cept⁻* +pXNG4-*CEPT* (blue square)
- *cept⁻* +pXNG4-*CEPT* GCV (magenta square)

B R2: 0.1%
R1 - cln#2-2-4 cept- -pXNG4CEPT(2)

C R2: 93.1%
R1 - cln#2-2-4 cept- -pXNG4CEPT(2)

D R2: 47.3%
R1 - cln#2-2-3 clone A cept- -pXNG4CEPT(2)

E R2: 31.7%
R1 - cln#2-2-4 clone B cept- -pXNG4CEPT(3)

F R2: 34.9%

GFP

G

pXNG copy #/cell

- *cept⁻* +pXNG4-*CEPT* SAT (**C**) (black)
- *cept⁻* +pXNG4-*CEPT* GCV (**D**) (red)
- Sorted GFP-high *cept⁻* +pXNG4-*CEPT* (green)
- Sorted GFP-low *cept⁻* +pXNG4-*CEPT* (yellow)

** and * significance markers

D

Cells	Promastigotes (pXNG4-*CEPT* copy#/cell)	Amastigotes (pXNG4-*CEPT* copy#/cell)					
		6 weeks (PBS)	6 weeks (GCV)	8 weeks (PBS)	8 weeks (GCV)	9 weeks (PBS)	9 weeks (GCV)
CEPT+/- +pXNG4-*CEPT*	22.18 ± 5.62	0.18 ± 0.06	0.03 ± 0.01	0.08 ± 0.02	0.01 ± 0.005	0.003 ± 0.001	0.0018 ± 0.0006
cept⁻ +pXNG4-*CEPT*	19.17 ± 6.53	0.40 ± 0.02	0.07 ± 0.004	0.10 ± 0.017	0.01 ± 0.008	NA	NA

A

No drug

+ SAT

B From PBS-treated mice

No drug

C From GCV-treated mice

No drug

D

+ SAT

E

No growth for all

+ SAT

CEPT+/- +pXNG4-*CEPT*

cept⁻ +pXNG4-*CEPT*